

Two-Dimensional Electronic Spectroscopy Reveals the Dynamics of Phonon-Mediated Excitation Pathways in Semiconducting Single-Walled Carbon Nanotubes

Matt W. Graham,^{†,‡,§} Tessa R. Calhoun,^{†,‡,#} Alexander A. Green,[§] Mark C. Hersam,[§] and Graham R. Fleming*,^{†,‡}

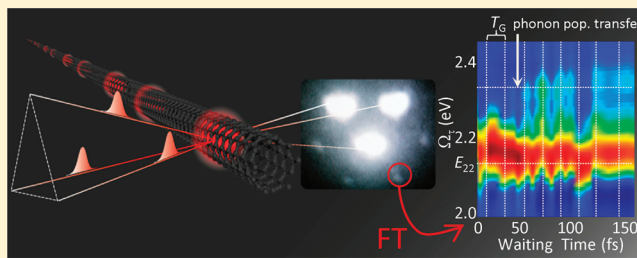
[†]Department of Chemistry, University of California, Berkeley, California 94720, United States

[‡]Physical Biosciences Division, Lawrence Berkeley National Laboratory, Berkeley, California 94720, United States

[§]Department of Materials Science and Engineering and Department of Chemistry, Northwestern University, Evanston, Illinois 60208, United States

ABSTRACT: Electronic two-dimensional Fourier transform (2D-FT) spectroscopy is applied to semiconducting single-walled carbon nanotubes and provides a spectral and time-domain map of exciton–phonon assisted excitations. Using 12 fs long pulses, we resolve side-bands above the E_{22} transition that correspond with the RBM, G, G', 2G and other multiphonon modes. The appearance of 2D-FT spectral cross-peaks explicitly resolves discrete phonon assisted population transfer that scatters excitations to the E_{22} (Γ -pt) state, often through a second-order exciton–phonon coupling process. All 2D-FT peaks exhibit a strong peak amplitude modulation at the G-band period (21 fs) which we show originates from an impulsive stimulated Raman process that populates a ground-state G-band vibrational coherence over a 1.3 ps phonon lifetime.

KEYWORDS: *ultrafast, carbon nanotubes, multidimensional spectroscopy, multiphonon assisted transition, phonon side-band, femtosecond dynamics*



The photophysics of semiconducting single-walled carbon nanotubes (SWNTs) are governed by quasi one-dimensional (1D) excitons whose confinement along the circumferential direction produces a sharp set of optical transitions (E_{11} , E_{22} , etc.) that scale inversely with tube diameter.^{1–3} Each optically bright exciton transition is further composed of a manifold of dark excitonic substates and bright phonon-assisted transitions. The resulting photoluminescence (PL) spectrum for even a single tube type (shown in Figure 1 for the (6, 5) tube) can be remarkably complex containing multiphonon, multiexciton and dark-state mediated transitions that are often obscured by strong excitation features.^{4,5} Contributions from such many body effects can produce very rapid relaxation over large energetic separations, making the determination of the overall optical relaxation pathways challenging. To provide the appropriate level of spectral and temporal resolution, we apply broadband 2D Fourier transform (2D-FT) electronic spectroscopy to semiconducting SWNTs.

Steady-state 2D-PL maps have been the predominant spectroscopic tool used in assigning SWNT chirality and surveying nanotube photophysics.^{5,6} As such, the ability to bring time-resolution to 2D spectral maps should provide new insight. In Figure 1a, the PL emitted from the (6, 5) E_{11} state is collected from an aqueous suspension of SWNTs as a 2D-PL map. Along the excitation axis, peaks correspond to the E_{22}

transition and a series of weaker E_{22} sideband states.⁷ The energetic spacing of the sideband peaks relative to the E_{22} transition match the ground state Raman modes indicated (white dotted lines) and are consistent with optical absorption via phonon side-bands.^{4,8–10} In particular, the E_{11} and E_{22} exciton states couple with several prominent phonon modes; including the tangential (G-band, 1590 cm^{-1}) and radial breathing mode (RBM for (6, 5), 296 cm^{-1}) motions along the carbon nanotube circumference (shown in Figure 2, top right).^{6,7,11}

Unlike bulk semiconductors, phonon-assisted absorption in SWNTs is greatly restricted by strongly correlated electron–hole (e–h) motions created from the powerful Coulombic attraction ($0.4\text{--}1\text{ eV} \gg k_B T$) caused by strong steric and screening constraints unique to this quasi-1D system.^{1,5} Consequently, each transition must conserve the center of mass momentum of the e–h pair (i.e., $\Delta K_{cm} \cong 0$), resulting in sharp excitonic peaks instead of the broad sloping phonon spectrum common to bulk semiconductors.⁷ For purely optical transitions such as E_{11} , E_{22} , and so forth, $\Delta K_{cm} \cong 0$ is satisfied by absorption near the Γ symmetry point of the SWNT

Received: November 2, 2011

Revised: December 19, 2011

Published: January 3, 2012

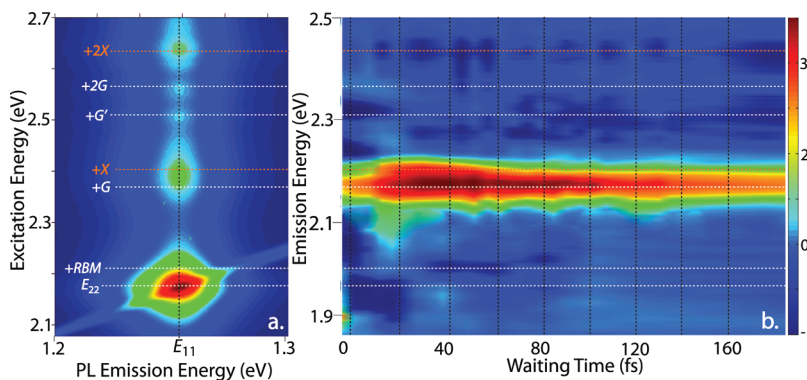


Figure 1. (a) The 2D-PL map of the E_{11} PL emission from the (6, 5) tube type after excitation of the E_{22} region. The dotted lines indicate E_{22} sideband peaks that match the labeled Raman modes (white) or strong excitation peaks (orange). (b) Frequency resolved pump–probe spectrum on the same sample reveals an oscillatory component with a ~ 21 fs period (vertical dashed black lines). Dashed horizontal lines along the induced absorption peaks (dark blue) show correspondence to the E_{22} sideband peaks labeled in (a) when an energetic offset of 1600 cm^{-1} (0.2 eV) is applied. Color scale bar is in $\Delta T/T$ (a.u.).

Brillouin zone. The state located “+G” above E_{22} is a one-phonon-assisted optical excitation and so can involve only zone-center phonons (i.e., $q_{\text{phonon}} \cong 0$) that return the exciton to the band edge.⁴ Alternatively, we can satisfy the $\Delta K_{\text{cm}} \cong 0$ restriction by the emission of two phonons of opposite momentum. For example, in Figure 1a we observe a distinct $+2G$ phonon sideband peak at 2.57 eV ($E_{22} + 2 \times 1590\text{ cm}^{-1}$).

Two further prominent E_{22} sideband peaks are indicated by orange dotted lines in Figure 1a. Possessing energies upshifted by $\sim 1930\text{ cm}^{-1}$ (labeled $+X$ at 2.4 eV) and $\sim 3850\text{ cm}^{-1}$ (labeled $+2X$ at 2.63 eV) they deviate significantly in frequency from their neighboring $+G$ and $+2G$ phonon sideband peaks. Proposed excitation mechanisms of the $+X$ sideband requires a two-phonon process that becomes favorable through involvement of two degenerate dark exciton states that possess center of mass momentum near the graphite K and K' symmetry points.^{7,9} Numerous 2D-PL studies have supported the involvement of these “so called” K -point states in the formation of phonon side-bands.^{4,7,12}

Phonon sideband peaks in SWNT excitation spectra are conventionally assigned by their energetic offset from the bright exciton. This presents two challenges; (a) the ground state and exciton state Raman frequencies may not be identical,^{8,11,13} and (b) spectral congestion often results in overlapping contributions. For instance, in Figure 1a the strongest sideband peak at 2.4 eV has a bandwidth roughly twice that of neighboring peaks. In this spectrum, we cannot clearly distinguish between one ($+G$) and multiphonon ($+X$) excitation pathways. Moreover, the energy spacing of both the $+X$ and $+2X$ peaks deviates significantly from known ground state Raman modes. To explain this result, second-order exciton–phonon coupling mechanisms involving the dark K -point exciton state have been invoked.^{7,14,15}

Ambiguity in peak assignment is further compounded by the intrinsically low PL yield for SWNTs and insensitivity to excitations that decay only through nonradiative pathways. To move beyond these limitations, and resolve complex phonon assisted excitations in SWNTs, 2D-FT electronic spectroscopy offers a distinct advantage. Specifically it provides an excitation (Ω_t) and emission (Ω_e) axis energy map of how an optical excitation distributes among allowed transitions over the course of electronic relaxation. 2D-FT spectroscopy combines the advantages of dual-axis spectral resolution like in 2D-PL SWNT

maps with the femtosecond time resolution of pump–probe spectroscopy.

We begin our time domain analysis of SWNT phonon sidebands by reporting a frequency resolved pump–probe spectrum (Figure 1b) on the same (6, 5) enriched SWNT sample used for the 2D-PL map. The prominent feature is the population relaxation of the E_{22} peak (2.16 eV) shown by positive (red) transient bleach decay. Our primary interest is the series of negative (dark blue) induced absorption peaks that appear at time intervals of roughly ~ 21 fs in Figure 1b. A similar pump–probe spectrum is reported by Luer et al. that resolves two broad induced absorption features adjacent to the E_{22} peak carefully assigned to phonon-assisted absorptions.¹⁶ Using broadband pulse compression techniques (see Experimental Methods),¹⁷ we achieve 12 fs long pulses that resolve a series of distinct induced absorption peaks. Strikingly, we find good correspondence between the E_{22} sideband peaks from the 2D-PL map in Figure 1a, and the spectrum of induced absorption peaks seen in the pump–probe spectrum (Figure 1b) when the two spectra are vertically offset by 1600 cm^{-1} ($\sim 0.2\text{ eV}$). This spectral offset and the 21 fs amplitude modulation observed correspond to the energy and period of the SWNT G-band Raman mode.¹⁸ Using 2D-FT electronic spectroscopy we will establish the mechanism relating Figures 1a and 1b to elucidate the formation and subsequent relaxation of the E_{22} phonon sidebands for (6, 5) chiral enriched SWNTs.

Our 2D-FT spectroscopy study uses $\sim 85\text{ nm}$ fwhm spectral dispersion corrected pulses centered at 2.3 or 2.0 eV to probe the E_{22} manifold of states for the dominant (6, 5) SWNT tube type. Using a nonlinear four-wave mixing process, three temporally delayed pulses excite the E_{22} region producing a stimulated photon echo response that has been previously observed in (6, 5) SWNTs at the E_{11} transition.¹⁹ For 2D-FT spectroscopy, the stimulated photon echo is collected as an interferogram using spectrally resolved heterodyne detection that preserves all amplitude and phase information. This interferogram is measured as a function of coherence time, τ (delay between pulses 1 and 2) and waiting times, T (delay between pulses 2 and 3, see Figure 2c inset). After a FT along the τ axis, the obtained real 2D spectra gives a sequence of maps showing differential absorption plotted as a function of excitation (Ω_t) and emission (Ω_e) energy at each waiting time (T) collected.²⁰

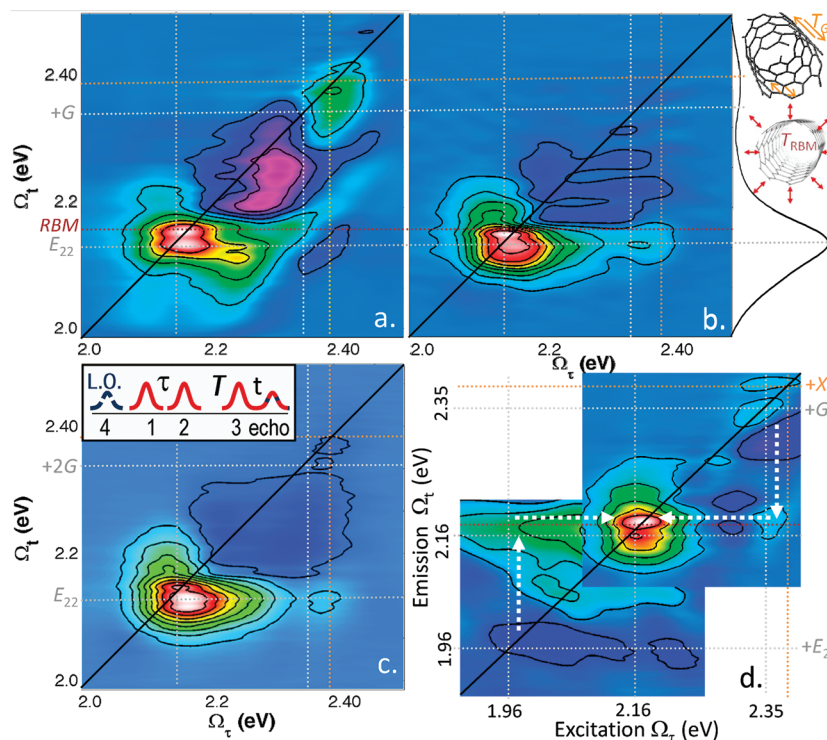


Figure 2. Real (6, 5) SWNT 2D FT relaxation spectra $S(\Omega_\tau, \Omega_v, T)$ for (a) $T = 0$ fs, (b) $T = 100$ fs, and (c) $T = 500$ fs. (d) $T = 20$ fs (showing both 2.3 and 2.0 eV excitation regions). Population transfer processes are indicated by the dashed arrows that link diagonal population states via their off-diagonal cross-peaks. Prominent phonon sideband peaks are labeled. Upper left inset in 2c shows pulse ordering of the three 12 fs pulses plus local oscillator (LO).

Previous SWNT ultrafast time-resolved studies typically use narrow band excitation and can resolve only the projection of a 2D-FT spectrum onto the Ω_τ axis. In addition to this enhanced spectral resolution, 2D maps produce “off-diagonal” cross-peaks that link two exciton states located along the “diagonal” line defined by $\Omega_\tau = \Omega_v$.²¹ Cross-peaks unambiguously show dynamic coupling or active population transfer between electronic and vibrational states of the same tube chirality. We capture the temporal evolution of all peaks and cross-peaks using 12 fs pulses. Such ultrafast precision resolves the exciton–phonon interaction directly as modulations in 2D-FT peak amplitudes that match the vibrational periods of the G-band ($T_G = 21$ fs) and (6, 5) RBM ($T_{RBM} = 110$ fs).

Representative real value 2D-FT spectra ($S(\Omega_\tau, \Omega_v, T)$) are plotted in Figure 2 for $T = 0, 100, 500$, and 20 fs, respectively. Positive (green to white) features correspond to transient bleaching or stimulated emission, while negative (dark blue to purple) features are induced absorptions. The dominant 2D-FT peak at $\Omega_\tau = \Omega_v = 2.16$ eV in Figure 2 is a strong transient bleach signal assigned to population relaxation from the E_{22} exciton state to the E_{11} state and other low lying states.^{16,22,23} In Figure 3a, the relaxation time ($T_{E_{22}}$) is obtained from both broadband (green circles, $\tau_{\text{pulse}} = 12$ fs), and narrow band (open orange circles, $\tau_{\text{pulse}} = 55$ fs) measurements that are resonant with the (6, 5) E_{22} transition. Using a least-squares deconvolution algorithm, the E_{22} bleach decays biexponentially (black line fit), giving a 120 fs (88%) E_{22} lifetime followed by a slower 1.25 ps (12%) component. While E_{22} relaxation times have been reported as short as 40 fs,^{24,25} our aqueous (6,5) sample gives a slightly longer decay (~120 fs) in accord with recent pump–probe simulations on this sample.²³

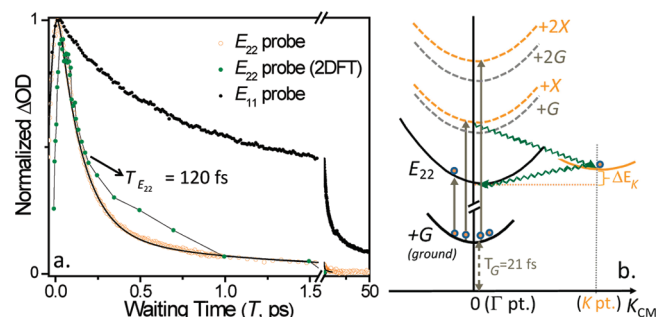


Figure 3. (a) Pump–probe time trace of kinetic relaxation of the (6, 5) E_{22} peak fitted to biexponential decay (black line). (b) Energy level diagram depicting induced absorption pathways from the ground-state G vibrational coherence populated by an impulsive stimulated Raman process. Excitation to the phonon sideband states (dashed lines) is accompanied by impulsive phonon emission (wavy lines) and transfer to the E_{22} state.

Along the diagonal line in Figure 2a,d we can identify the positive (6, 5) SWNT E_{22} peak at $\Omega_\tau = \Omega_v = 2.16$ eV, and two positive sideband peaks labeled +G and +X located ~1590 and ~1930 cm⁻¹ above E_{22} . These diagonal peaks match the steady-state linear absorption spectrum shown to the right of Figure 2b. In the $T = 0$ spectra, we believe the negative (purple) diagonal peak is largely an artifact of nonresonant contributions that can occur within the pulse overlap regions. Off-diagonal, cross-peaks show population transfer from the diagonal sideband peaks to the E_{22} exciton state (e.g., see Figure 2d).

For waiting times (T) far outside the pulse overlap region (e.g., Figure 2b,c) the positive diagonal sideband peaks seen for $T = 0$ and 20 fs are replaced by negative induced absorptions (dark blue). A broad multipeaked induced absorption feature

covering the diagonal region from ~ 2.2 to 2.3 eV is also resolved. Similar to the pump–probe spectrum in Figure 1b, we find the 2D-FT induced absorption peaks along the diagonal line also match the 2D-PL excitation spectrum when a spectral offset of ~ 1600 cm $^{-1}$ is applied. This persistent offset suggests the negative (dark blue) peaks arise from an induced absorption from the ground state G-band mode as depicted in Figure 3b.

To show the time evolution of 2D-FT cross-peaks alongside the E_{22} diagonal peaks, we take vertical (emission axis, Figure 4a,b) and horizontal (excitation axis, Figure 4c,d) cuts through the real 2D-FT spectra and plot these cuts as a function of T .

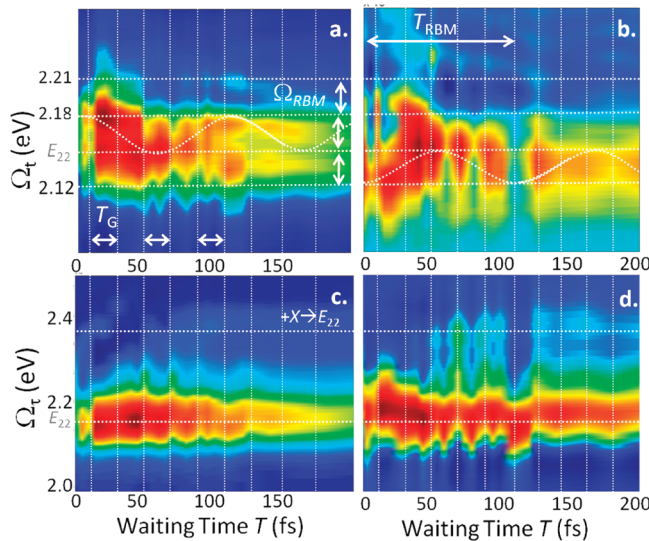


Figure 4. (a) Time evolution of vertical line-cuts taken from 2D-FT relaxation spectra at $\Omega_t = 2.17$ eV. A sinusoidal oscillation one Ω_{RBM} frequency above E_{22} is indicated. (b) Line-cuts for the corresponding NR spectra at $\Omega_t = 2.25$ eV show a similar oscillation one Ω_{RBM} frequency below E_{22} . (c) Time-evolution of horizontal line-cuts along the excitation axis for $\Omega_t = 2.16$ eV. (d) Corresponding NR spectrum. The labeled $+X \rightarrow E_{22}$ feature is a cross-peak showing the population transfer from a $+X$ or $+2X$ phonon sideband to E_{22} . Dotted lines guide the eye to frequency modulations at the RBM (± 0.035 eV) and amplitude modulations at G-band period (21 fs).

Vertical dashed lines placed at 21 fs (T_G) intervals highlight strong amplitude modulations, whose period closely corresponds to the G-band mode. A secondary amplitude (every ~ 110 fs) and frequency modulation (± 280 cm $^{-1}$) are indicated by dotted sinusoidal lines in Figure 4a,b, and closely correspond to the (6, 5) RBM mode of 296 cm $^{-1}$.¹⁸ Such oscillatory behavior indicates an impulsive wave packet excitation with an ultrashort pulse creating a vibrational superposition between the E_{22} and a RBM phonon sideband.^{26–28}

Below E_{22} , we find a symmetric RBM oscillation is prominent when we instead plot just the nonrephasing (NR) component of the real 2D-FT spectra (Figure 4b). The NR spectrum uses data acquired from $\tau = -200$ to 0 fs only. This effectively swaps the pulse ordering shown in Figure 2c (inset) and provides an enhanced resolution of antidiagonal (inhomogeneous) spectral broadening contributions.^{21,29} The resulting NR spectral line cuts show a second RBM oscillation one Ω_{RBM} below the E_{22} transition. We also detect signatures of a RBM overtone mode at $\Omega_t = 2.21$ eV or $E_{22} + 2 \times \text{RBM}$ in Figure 4a,b. The guiding sinusoidal lines further show a relative π phase shift in the

vibrational coherence of the \pm RBM phonon sidebands. A similar E_{22} RBM π -phase shift has been previously extracted from optical pump–probe spectra.¹⁶

Figures 4c,d and 5a highlight the time-dependent behavior of select 2D-FT cross-peaks. We plot the evolution of the $+X \rightarrow E_{22}$ cross-peak alongside the diagonal E_{22} peak through cuts

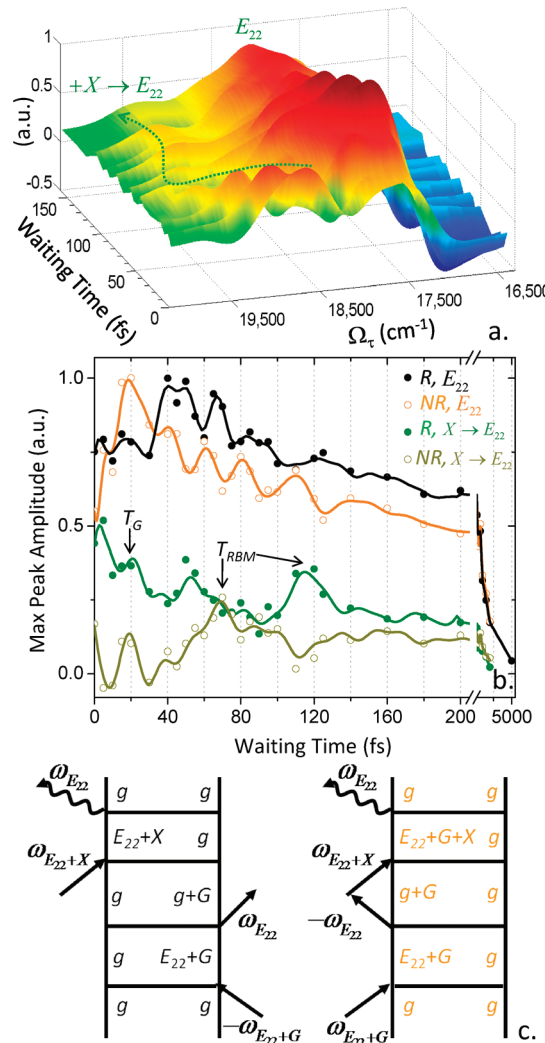


Figure 5. (a) A line-cut along the excitation axis of 2D-FT rephasing spectra at $\Omega_t = 2.19$ eV (E_{22} peak) shows the time evolution of the E_{22} peak and its corresponding $+X \rightarrow E_{22}$ cross-peak. (b) The maximum 2D-FT peak amplitude in region of the E_{22} transition and cross-peak is plotted as function of waiting time. The R and NR contributions are anticorrelated outside the pulse overlap region. (c) Feynman pathways for a stimulated Raman process that creates a G-band vibrational coherence that give nonequivalent induced absorption pathways for the R (black) and NR (orange) excitation pathways producing the cross-peaks shown above in 5a,b.

taken along the (horizontal) excitation axis at $\Omega_t = 2.16$ eV. While the cross-peak feature shown in Figure 4c appears weak, we find it is markedly enhanced when the NR ($\tau < 0$, Figure 4d) and rephasing (R , $\tau > 0$, Figure 5a) contributions of total real 2D-FT signal are plotted separately.

All resolvable 2D-FT peaks exhibit persistent amplitude modulations at 21 fs (T_G) for the first 200 fs (see Figures 4 and 5) after which the time points were too sparsely sampled. Such an amplitude modulation pattern is consistent with a

vibrationally coherent wavepacket on the ground state created by an impulsive stimulated Raman process involving the G-band (see Figure 3b).²⁶ In Figure 5b, we plot the peak amplitude modulations of the R and NR excitation pathways and show they are anticorrelated outside the pulse overlap region. Existing time-resolved measurements can resolve only the summation of R + NR contributions. Figure 5b shows how the separation of the two excitation pathways provide an enhanced resolution to phonon-mediated population processes, that will give us the ability to identify exciton sideband peaks that arise from second-order exciton–phonon coupling.

The 2D-FT spectral cross-peaks explicitly show impulsive population transfer from phonon sidebands to the bright E_{22} state. As such, the cross-peaks shown in Figures 2, 4, and 5 show dominant (6, 5) SWNT phonon sidebands (e.g., $+X/+2X$) are bound to the E_{22} exciton state. Comparing Figures 4d and 5a, we further see that both diagonal and cross peaks exhibit a secondary frequency oscillation along the Ω_r axis at $\sim 290 \text{ cm}^{-1}$ (Ω_{RBM}) at $\sim 110 \text{ fs}$ (T_{RBM}). In Figure 5b, the modulation pattern is numerically extracted by plotting the maximum real 2DFT amplitudes of the E_{22} peak and the $X \rightarrow E_{22}$ cross-peak. Fitting using singular value decomposition (solid lines) we obtain frequencies (and % amplitudes) that closely match the phonon modes indicated at $1580 \pm 22 \text{ cm}^{-1}$ (G, 63%), $290 \pm 44 \text{ cm}^{-1}$ (RBM, 25%) and $1176 \pm 30 \text{ cm}^{-1}$ (12%). The $+X \rightarrow E_{22}$ cross-peak is strongly modulated along the excitation axis at both the G band and RBM frequencies showing that multiple phonon modes are used to satisfy the $K_{\text{cm}} \cong 0$ restriction for exciton formation.

2D-FT spectroscopy on semiconducting SWNTs provides a time-domain mapping of excitation and relaxation pathways involving the phonon sidebands of the (6, 5) E_{22} exciton. We find the E_{22} sideband peaks seen in our pump–probe and 2D-FT show good spectral agreement to the 2D-PL map after an offset matching the G-band frequency is applied (Figures 1a,b and 2). Our strongest sideband peaks denoted $+X$ and $+2X$, deviate from the expected $+G$ and $+2G$ phonon-side bands by 23 and 45 meV, respectively. Such deviations have been previously seen in steady-state measurements^{7,12,14} and explained through emission of two phonons which satisfy $\Delta K_{\text{cm}} \cong 0$ rule for bright exciton creation (e.g., the two wavy arrows in Figure 3b). This second-order exciton–phonon coupling process is enhanced by strong phonon scattering processes expected at the K-point.^{4,7,8} Our time-resolved results support that such multiphonon assisted excitations are often stronger than other one-phonon processes observed (e.g., $+G$ and $+G'$). However, we can only infer the potential involvement of the K-point state by noting the energetic displacement of the $+X$ and $+2X$ peaks. This would place the dark K-point state ~ 23 meV above E_{22} . Previous values for the E_{11} K-point state have been reported, ranging from 12 to 50 meV.^{7,30}

The $+X$ or $+2X \rightarrow E_{22}$ cross peak decays with a lifetime of 1.3 ps, similar to the recently reported 1.1 ± 0.2 ps ground state G phonon lifetime.^{28,31} The cross-peak lifetime and its strong 21 fs beat period (T_G) further coincide with the mechanism outlined in Figure 3b whereby the induced absorption peaks in Figures 1b and 2 originate from a vibrational coherence with the ground state G-band produced by a stimulated Raman process. This impulsive stimulated Raman excitation mechanism is made explicit in Figure 5c with representative double-sided Feynman diagrams for the R and NR 2D-FT spectra. These diagrams depict the time evolution of the density matrix for the four-wave mixing stimulated Raman process and

subsequent induced absorption to either an $+X$ or $+2X$ phonon-sideband state that give rise to the observed cross-peaks in Figure 5a,b. The first two arrowed interactions ($\pm \omega_{E_{22}}$) impulsively stimulate a vibrational superposition (i.e., $|g\rangle\langle g + G\rangle$) that beats every 21 fs (T_G period). Alternately, stimulated Raman scattering can occur from other bound exciton states such as E_{22} and $E_{22}+X$ (not shown). After the waiting time T , the third pulse produces the induced absorption peaks seen throughout our 2D-FT spectra. For simplicity, Feynman pathways show only optical interactions, relaxation by phonon emission is implicit.

The Feynman diagram description of the stimulated Raman process is also helpful to explain why the R and NR pathways result in a clear π -phase shift in peak amplitude (Figures 4d and 5a,b). The third pulse interaction (see Figure 5c) only excites population in the G-band state through the NR pathway. In the R pathway, the corresponding interaction occurs with the $|g\rangle$ state. However, as time (T) evolves the G-band vibrational superposition beats. Every period $T = nT_G/2$, the G population will effectively swap whether the indicated induced absorption occurs in the R or NR 2D-FT pathway. Consequently, we observe the peak and cross-peak modulations in Figure 5b are anticorrelated (or π -phase shifted) for both G-band and RBM periods.

We demonstrate the application of 2D-FT electronic spectroscopy to semiconducting SWNTs to obtain a time-dependent spectral map of phonon-assisted absorption peaks of the E_{22} transition in the (6, 5) tube type. Broadband excitation with 12 fs pulses creates a stimulated Raman population of the G-band via the E_{22} phonon side-bands. A resulting ground-state vibrational coherence is observed through induced absorption peaks that match the 2D-PL spectrum of phonon sidebands but are downshifted by the G-band frequency. The strong anticorrelated peak amplitude modulations at the 21 fs G-band period originate from a stimulated Raman process. Through induced absorption from the ground state G-band vibrational coherence, we continue to repopulate the E_{22} state for the 1.3 ps G-band lifetime.

A unique contribution from 2D-FT spectroscopy is the resolution of cross-peak contributions. Cross-peaks clearly show population transfer $+X \rightarrow E_{22}$ and $+2X \rightarrow E_{22}$ via phonon emission, demonstrating that such phonon sideband states are indeed bound to the singlet E_{22} exciton. We find that the cross peak modulates in both amplitude and frequency at the G-band and RBM, showing the strongest E_{22} phonon sidebands involve multiple-phonon emission. We suspect that such a second-order exciton–phonon coupling process is made favorable because of enhanced coupling at a dark K-point state that would lie ~ 23 meV above the E_{22} transition. Similar population exchange processes are also expected for the E_{11} transition, and future analogous E_{11} 2D-FT maps should provide a complete dynamic map of the still nebulous nonradiative decay pathways for semiconducting SWNTs.

Experimental Methods. The SWNT sample was synthesized through the cobalt molybdenum catalyst (CoMoCAT) technique, dispersed in surfactants, and then greatly enriched in the (6, 5) semiconducting tube type through a density-gradient ultracentrifugation process.^{32,33} The resulting aqueous suspension of individually separated SWNTs enabled resonant excitation of predominately the (6, 5) tube type. In order to suppress laser light scattering, a thin 100 μm path length quartz cell was used with a sample optical density of 0.12 at 571 nm. PL absorption measurements were taken on a Jobin-Yvon

Fluorolog using 150 W xenon arc lamp excitation and a Li–N₂ cooled CCD camera and InGaAs photodiode. Measurements were conducted under ambient conditions since the absorption line shape is dominated by inhomogeneous broadening,³⁴ meaning low-temperature measurements only modestly reduce spectral congestion.

Broadband (\sim 85 nm fwhm) pulses centered at 2.3 or 2.0 eV were generated from a noncollinear optical parametric amplifier (NOPA) pumped by home-built 3.4 kHz Ti:sapphire/regenerative amplifier system. The 2D-FT technique used is described in detail elsewhere.^{20,21,35} Briefly, the beam was split into two paths and temporally offset with a mechanical delay stage (Newport, UTS series) to control the waiting time (T). A diffractive optic further splits each path to produce the requisite phase-locked pulse pairs (see Figure 2c, inset). The coherence time (τ) delay was introduced through fused silica glass wedges on delay stages (Nanomovers, Melles-Girot), that were temporally calibrated using spectral interferometry. The laser pulses were compressed to 12 fs with a prism pair to correct for the quadratic-order spectral phase and spatial light-modulator (SLM) line to correct for high-order spectral phase contributions. Transient-grating frequency resolved optical gating (TG-FROG) was preformed on fused silica at the sample position to extract the phase necessary to create a compressed, virtually unchirped pulse.¹⁷

The pulse-pairs were focused on the SWNT sample in a box geometry with a total incident fluence of 2.3×10^{14} and 3.4×10^{14} photons/cm² for the 2.0 and 2.3 eV centered experiments respectively. A heterodyne detection scheme on CCD camera (Princeton Instruments) was accomplished by passing the fourth LO pulse collinear with the emitted signal (k_s). This enabled us to spectrally resolve the SWNT signal collected in the $k_s = -k_1 + k_2 + k_3$ phase matched direction in both amplitude and phase. The data were collected at waiting times from 0 to 5000 fs. For each waiting time, the coherence time was scanned from –200 to 200 at 5 fs increments. A Fourier transform over the τ -axis generates the absorption energy axis (Ω_τ). Spectrally resolved pump–probe taken immediately after was used to phase the absolute values in 2D spectra obtained. These spectra are plotted in Figure 1b.

To exclude potential contributions from local heating and sample degradation, the 2D-FT experiment was repeated by flowing the aqueous tube suspension or using a thin SWNT–polymer composite of polyvinylpyrrolidone (PVP) polymer. While the signal-to-noise deteriorated from scattering, the same 2D-FT features were still prominent. Similar 2D-FT spectral features were observed at all excitation fluences examined (0.6 – 6.2×10^{14} photons/cm²).

AUTHOR INFORMATION

Corresponding Author

*E-mail: grfleming@lbl.gov.

Present Addresses

¹Kavli Institute at Cornell for Nanoscale Science, Cornell University, Ithaca, NY, 14850, United States.

[#]Lewis-Sigler Institute for Integrative Genomics, Princeton University, Princeton, NJ, 08544, United States.

ACKNOWLEDGMENTS

This work is supported by NSF Grant CHE-1012168 to G.R.F. M.W.G. and A.A.G. thank Natural Sciences and Engineering Research Council of Canada for postgraduate scholarships.

Density gradient processing was supported by the NSF (DMR-1006391 and DMR-1121262) and the Nanoelectronics Research Initiative. We thank Y.-Z. Ma, G. S. Schlau-Cohen, and L. V. Valkunas for their helpful contributions.

REFERENCES

- (1) Wang, F.; Dukovic, G.; Brus, L. E.; Heinz, T. F. *Science* **2005**, *308* (5723), 838–841.
- (2) Maultzsch, J.; Pomraenke, R.; Reich, S.; Chang, E.; Prezzi, D.; Ruini, A.; Molinari, E.; Strano, M.; Thomsen, C.; Lienau, C. *Phys. Rev. B* **2005**, *72*, 241402(R).
- (3) Ma, Y.-Z.; Valkunas, L.; Bachilo, S. M.; Fleming, G. R. *J. Phys. Chem. B* **2005**, *109* (33), 15671–15674.
- (4) Chou, S. G.; Plentz, F.; Jiang, J.; Saito, R.; Nezich, D.; Ribeiro, H. B.; Jorio, A.; Pimenta, M. A.; Samsonidze, G. G.; Santos, A. P.; Zheng, M.; Onoa, G. B.; Semke, E. D.; Dresselhaus, G.; Dresselhaus, M. S. *Phys. Rev. Lett.* **2005**, *94* (12), 127402.
- (5) Dresselhaus, M.; Dresselhaus, G.; Saito, R.; Jorio, A. *Annu. Rev. Phys. Chem.* **2007**, *58*, 719–747.
- (6) Bachilo, S.; Strano, M.; Kittrell, C.; Hauge, R.; Smalley, R.; Weisman, R. *Science* **2002**, *298*, 2361–2366.
- (7) Torrens, O. N.; Zheng, M.; Kikkawa, J. M. *Phys. Rev. Lett.* **2008**, *101* (15), 157401.
- (8) Perebeinos, V.; Avouris, P. *Phys. Rev. Lett.* **2005**, *94*, 027402–027402.
- (9) Plentz, F.; Ribeiro, H.; Jorio, A.; Strano, M.; Pimenta, M. *Phys. Rev. Lett.* **2005**, *95*, 247401–247401.
- (10) Lebedkin, S.; Hennrich, F.; Kiowski, O.; Kappes, M. M. *Phys. Rev. B* **2008**, *77* (16), 165429.
- (11) Tretiak, S.; Kilina, S.; Piryatinski, A.; Saxena, A.; Martin, R. L.; Bishop, A. R. *Nano Lett.* **2006**, *7* (1), 86–92.
- (12) Miyauchi, Y.; Maruyama, S. *Phys. Rev. B* **2006**, *74* (3), 035415.
- (13) Ma, Y.-Z.; Graham, M. W.; Prantil, M. A.; Van Tassel, A. J.; Fleming, G. R. *J. Phys. Chem. B* **2008**, *112* (50), 16030–16034.
- (14) Vora, P. M.; Tu, X.; Mele, E. J.; Zheng, M.; Kikkawa, J. M. *Phys. Rev. B* **2010**, *81* (15), 155123.
- (15) Matsunaga, R.; Matsuda, K.; Kanemitsu, Y. *Phys. Rev. B* **2010**, *81* (3), 033401.
- (16) Luer, L.; Gadermaier, C.; Crochet, J.; Hertel, T.; Brida, D.; Lanzani, G. *Phys. Rev. Lett.* **2009**, *102* (12), 127401–4.
- (17) Vaughan, J. C.; Hornung, T.; Feurer, T.; Nelson, K. A. *Opt. Lett.* **2005**, *30* (3), 323–325.
- (18) Jorio, A.; Dresselhaus, M. S.; Saito, R.; Dresselhaus, G. *Raman Spectroscopy in Graphene Related Systems*; John Wiley & Sons: New York, 2011.
- (19) Graham, M. W.; Ma, Y.-Z.; Fleming, G. R. *Nano Lett.* **2008**, *8* (11), 3936–3941.
- (20) Brixner, T.; Mancal, T.; Stiopkin, I. V.; Fleming, G. R. *J. Chem. Phys.* **2004**, *121* (9), 4221.
- (21) Cho, M. *Chem. Rev.* **2008**, *108* (4), 1331–1418.
- (22) Zhu, Z.; Crochet, J.; Arnold, M. S.; Hersam, M. C.; Ullbricht, H.; Resasco, D.; Hertel, T. *J. Phys. Chem. C* **2007**, *111* (10), 3831–3835.
- (23) Graham, M. W.; Chmeliov, J.; Ma, Y.; Shinohara, H.; Green, A. A.; Hersam, M. C.; Valkunas, L.; Fleming, G. R. *J. Phys. Chem. B* **2011**, *115* (18), 5201–5211.
- (24) Manzoni, C.; Gambetta, A.; Menna, E.; Meneghetti, M.; Lanzani, G.; Cerullo, G. *Phys. Rev. Lett.* **2005**, *94* (20), 207401.
- (25) Gambetta, A.; Manzoni, C.; Menna, E.; Meneghetti, M.; Cerullo, G.; Lanzani, G.; Tretiak, S.; Piryatinski, A.; Saxena, A.; Martin, R.; Bishop, A. *Nat. Phys.* **2006**, *2* (8), 515–520.
- (26) Pollard, W. T.; Lee, S.; Mathies, R. A. *J. Chem. Phys.* **1990**, *92* (7), 4012.
- (27) Luer, L.; Gadermaier, C.; Crochet, J.; Hertel, T.; Brida, D.; Lanzani, G. *Phys. Rev. Lett.* **2009**, *102* (12), 127401.
- (28) Song, D.; Wang, F.; Dukovic, G.; Zheng, M.; Semke, E. D.; Brus, L. E.; Heinz, T. F. *Phys. Rev. Lett.* **2008**, *100* (22), 225503.

- (29) Nemeth, A.; Milota, F.; Mancal, T.; Pullerits, T.; Sperling, J.; Hauer, J.; Kauffmann, H. F.; Christensson, N. *J. Chem. Phys.* **2010**, *133*, 094505.
- (30) Capaz, R.; Spataru, C.; Ismail-Beigi, S.; Louie, S. *Phys. Rev. B* **2006**, *74*, 121401(R)–121401(R).
- (31) Kang, K.; Ozel, T.; Cahill, D. G.; Shim, M. *Nano Lett.* **2008**, *8* (12), 4642–4647.
- (32) Arnold, M. S.; Green, A. A.; Hulvat, J. F.; Stupp, S. I.; Hersam, M. C. *Nat. Nanotechnol.* **2006**, *1*, 60–65.
- (33) Green, A. A.; Hersam, M. C. *Adv. Mater.* **2011**, *23* (19), 2185–2190.
- (34) Graham, M. W.; Ma, Y.-Z.; Green, A. A.; Hersam, M. C.; Fleming, G. R. *J. Chem. Phys.* **2011**, *134*, 034504.
- (35) Ginsberg, N. S.; Cheng, Y.; Fleming, G. R. *Acc. Chem. Res.* **2009**, *42* (9), 1352–1363.